MOBILE MAPPING SYSTEMS AND SPATIAL DATA COLLECTION STRATEGIES ASSESSMENT IN THE IDENTIFICATION OF HORIZONTAL ALIGNMENT OF HIGHWAYS

Marinelli, G., Bassani, M. (*), Piras, M., Lingua, A. M.

Giuseppe Marinelli
Post-doctoral fellow
NTNU - Norwegian University of Science and Technology,
Department of Civil and Environmental Engineering
Faculty of Engineering
Høgskoleringen 7A
7491, Trondheim, Norway
Phone: +47 468 23 584
E-mail: giuseppe.marinelli@ntnu.no

Marco Bassani (* = *corresponding author*)
Associate Professor
Politecnico di Torino
Department of Environment, Land and Infrastructures Engineering (DIATI)
24, corso Duca degli Abruzzi
Torino, Italy, 10129
Phone: +39 011 090 5635
E-mail: marco.bassani@polito.it

Marco Piras
Associate professor
Politecnico di Torino
Department of Environment, Land and Infrastructures Engineering (DIATI)
24, corso Duca degli Abruzzi
Torino, Italy, 10129
Phone: +39 011 090 7661
E-mail: marco.piras@polito.it

Andrea M. Lingua
Associate Professor
Politecnico di Torino
Department of Environment, Land and Infrastructures Engineering (DIATI)
24, corso Duca degli Abruzzi
Torino, Italy, 10129
Phone: +39 011 090 7700
e-mail: andrea.lingua@polito.it

ABSTRACT

The horizontal alignment of existing highways may be identified by using several terrestrial or aerial geomatics technologies. Such technologies involve different levels of precision and accuracy; hence, different results can be expected. At present, there are no comparisons available between the solutions resulting from the use of different technologies and data sources for the same road alignment.

In this investigation, a number of terrestrial mobile mapping techniques and data collection strategies were evaluated. The centerline of a 3.6 km section of a highway was used to estimate radii, centers of curvature and orientation of tangents. Two statistical fitting methods were used to back-calculate these parameters, and the results were then compared with as-built alignment data.

Terrestrial images from a mobile mapping vehicle were used to determine the centerline, which was also estimated as the average line of the carriageway and pavement edges, and as the average line of the two driving trajectories. Positions were surveyed using low-cost sensors (an integrated GPS-IMU platform, HD webcam). For comparison purposes, aerial orthophotos and a GNSS (high-cost) receiver were used simultaneously. Although the GPS-IMU data and estimated trajectories provided results comparable to those of the GNSS receiver, the use of georeferenced images proved less accurate. The results and comments in the paper should be of use to survey practitioners when they need to select an acquisition methodology appropriate to the desired level of accuracy and in line with budget constraints.

KEYWORDS:

horizontal alignment

geometric identification

geographic information system

inertial sensors

global navigation satellite system

low-cost sensors

as-built project

1. INTRODUCTION

For several reasons, engineers need to establish the geometric characteristics of the elements forming the alignment of existing roads. This happens in the case of cadastral and surveying operations, to support safety and human factor studies, to control the quality of road construction, and more recently, in automotive engineering for Advanced Driver Assistance Systems (ADAS) and driverless vehicle applications.

Alignment identification consists of procedures aimed at the back-calculation of the geometric characteristics of the road from the collection of geospatial data of the road centerline. For some of the abovementioned applications, obtaining a precise spatial location of the various road elements (i.e., point of curvature, curve termini, vertexes), is less important than the estimation of geometric characteristics such as tangent orientation and length, radius of curvature, and spiral transition scale factor.

Road agencies do not always have complete geometric information on their infrastructures. In Italy, more than 85% of the 500,000 km network of existing roads was built before 1980 (Benedetto, 2000), the year in which CAD software was first used on microcomputers and employed in road design. Hence, alignment data information is unavailable for most existing roads. When available, the data are often reported in project drawings, thus time and effort are necessary to retrieve them in a format useful for numerical analysis and modelling. Furthermore, they may also differ from the actual current layout due to changes resulting from maintenance or reconstruction activity.

Engineers design the road alignment as a sequence of straight and curved elements. Following construction, a dedicated survey is usually carried out to determine the as-built alignment, which indicates the final position of the road on the ground. Any differences between the designed and as-built road alignments are attributable to inaccuracies of survey devices and construction operations. In addition, the as-built alignment is commonly assumed as coinciding with the road centerline marking, which in turn does not correspond to the designed roadway mid-line as a consequence of the inevitable distortions caused by laying operations. To avoid any erroneous evaluations, the as-built alignment may also be obtained by recourse to different strategies, i.e. averaging parallel lines that either delimit the roadway (both pavement or carriageway edges), or that are derived from the trajectories of survey vehicles collected by means of Mobile Mapping (MM) technologies.

The use of MM is promoted by many road agencies since data can be collected in a short time and updated very quickly (Findley et al., 2011). Alternatively, spatial data can also be collected from the interpretation of digital maps and aerial images, also using GIS tools.

All these technologies involve different levels of precision and accuracy; therefore, when employed in the identification of the horizontal alignment, different results can be expected. At present, there are no comparisons available between the alignment solutions resulting from the use of different spatial data sources for the same road alignment.

The aim of the research was to test, evaluate, and compare different methodologies in terms of the survey devices (using both low and high-cost sensors), fitting algorithms and data sources used to calculate the center of curvature location and radius, as well as tangent direction of existing roads. This objective was pursued with the back-analysis of geospatial data points of the centerline marking, and also employed different strategies by averaging the survey vehicle trajectories in the two directions, as well as the two carriageway and two pavement edges.

Data was collected on a section of a two-lane rural road in the Northwest of Italy. The alignment of this section is characterized by combined curves (circular arcs with transition clothoids) with radii of 550 m and with different lengths and central angles. Data validation, by means of reference to the as-built project drawings, was carried out to verify the accuracy of the proposed data collection method.

2. RELATED WORK

One way to obtain spatial information on the horizontal alignment of roads is to use Mobile Mapping (MM) technologies (Harkey et al., 2004), where vehicles with sensors on board such as Global Navigation Satellite Systems (GNSS), laser scanners (LiDAR), digital cameras, Inertial Measurement Units (IMU), and integrated devices (i.e., GNSS-IMU) are used to collect spatial data (position, attitude, images and point clouds) while travelling along a road.

For this purpose, GNSS and IMU sensors have been employed by several authors to measure the vehicle trajectory or the position of the horizontal marking, which many assume to represent the centerline in the cross-section (Ai and Tsai, 2014). Geo-referenced imagery from digital cameras on MM vehicles were proposed for the detection of lane markings (López et al., 2010), and/or for the extraction of information to support road inventory activities (de Frutos and Castro, 2014). The level of accuracy attainable using these systems can range from centimeters to meters, depending on the technology used and the quality of the output signal.

Some of the past contributions to the detection of the horizontal alignment were made by averaging the data points collected along the two driving trajectories. In these

contributions, it was assumed that the data collected along each path were located approximately in a symmetrical pattern with respect to the centerline. Drakopoulos and Örnek (2000) considered the quality of the extracted geometric information from Global Positioning System (GPS) surveys acceptable following a comparison with as-built data. The methodology was applied to a two-lane highway and proved effective even in the case of short curves with small deflection angles. Some difficulties arose with the identification of curves shorter than 300 m.

Crisman and Robba (2004) compared as-built data with those derived from the analysis of data collected by the MM vehicle. In the case of tangents and circular arcs, they observed good compliance, while in the case of spirals they concluded that the length and scale parameters were too sensitive to small differences between calculated and real values, thus leading to unsuccessful results even in the case of circular arcs with large radii and of short length. Choi and Sung (2006) corroborated this result since they found that the estimate of the clothoid scale parameter had a higher error range when compared with the geometric characteristics of tangents and circular arcs.

Castro et al. (2006) compared the two curvature diagrams obtained from the highway alignment defined by parametric cubic smoothing splines and project alignment, and found that the maximum error in the definition of the roadway alignment was equal to 1 m, a value that they considered satisfactory for topographical representation and highway applications. Imran et al. (2006) also collected data using a differential GPS surveying method along a 25 km section of a two-lane rural highway in eastern Ontario. Curve radii values ranged from 349.00 to 873.20 m, with curve length between 162.40 and 783.64 m. Integration into a Geographic Information System (GIS) environment enabled the utilization of GIS capabilities including map and graphical displays and the ability to integrate the fitted alignment with available digital maps. This GPS/GIS based method allowed an accurate determination of the radii of the highway alignment with an average difference of only 1.55% between the observed and actual values.

Roh et al. (2003) analyzed the centerline obtained by fixing the GNSS receivers to the center of a pallet, which was pulled manually along the centerline and lane markings. They did not use MM vehicles since they were convinced that different driving patterns would have a disproportionate influence on surveyed values.

There has been a significant number of research investigations into vision-based road lane detection and tracking focused on road survey activity, traffic monitoring, and driverless vehicle guidance (Ishikawa and Kuwamoto, 1988; Jochem et al., 1988; Hu and Uchimura,

1999; Beauvais and Lakshmanan, 2000; McCall and Trivedi, 2004; Tai et al., 2004; Toth and Grejner-Brzezinska, 2004; Choi and Lee, 2006; Guan et al, 2014; Holgado-Branco et al., 2015). Some works have focused on lane extraction in image sequences using geo-referenced information from other sensing devices (i.e., GNSS, IMU). Tao et al. (2001) extracted a 3D model of the centerline using an edge detection gradient algorithm, McCall and Trivedi (2004) resolved the lane detection problem using steerable filters (Freeman and Adelson, 1991), while Li et al. (2004) and Roncella and Forlani (2006) detected the white line and road boundaries by means of Hough transform (1959) applied to Sobel masked images.

Two significant contributions to road surveys producing high-precision "as-built" plans came from Toth and Grejner-Brzezinska (2004), who used a purpose built van-based integrated mapping system composed of a high precision integrated GPS/INS navigation system and a fully digitalized and automated imaging subsystem, and from Holgado-Barco et al. (2015) who employed an integrated capture system made up of a navigation system, two LiDAR sensors, and four RGB cameras. Both systems were set to detect the road centerline with sensors mounted vertically and facing downwards. A dataset of spatial points can be collected using a terrestrial or an aerial system. The former consists of one or more sensors mounted on an MMS and coupled with a GNSS/INS system to geo-reference the spatial data. The latter is installed on a plane, helicopter, or a drone (Lin et al. 2011), and is also coupled with a geo-referencing system (i.e., GNSS/INS).

A preference for the vision-based system over the laser-based surveying methodology can be attributed to its greater potential and fewer limitations. LiDAR is a powerful system which can collect a vast quantity of discrete and irregular spatial data and which takes advantage of the reflectance of the surveyed points. In contrast, image and photogrammetric techniques lead to the collection of continuous spatial elements that need to be extracted (automatically or manually) and that can be detected by exploiting both the radiometry and reflectance properties of objects captured in the frames.

LiDAR data (point clouds) can be automatically classified and used to extract multiple road elements. The classification of data can be carried out by considering the reflectivity index of the single point. Moreover, each point cloud can be coupled with an image to generate a colored cloud. The color may also be used to classify points. LiDAR data acquisition is faster than other Geomatics techniques, but the data processing requires more time to filter the point clouds. It is also necessary to remove outliers. On the other hand, LiDAR data management is more complex with respect to the other methods, because of the large amount of data involved (sometimes composed of millions of points).

As for image analysis, Tarel et al. (2007) formulated a new algorithm for two-image alignments by considering edge images. In particular, they employed this alignment algorithm for the off-line longitudinal road profile reconstruction from stereo images. More recently, Cheng et al. (2008) developed an automatic extraction system for the post-processing of geo-referenced images captured by a land-based MM system. The input of the system is the MM data acquired using VISAT, a commercial, high-cost MM that includes a GNSS-IMU system (usually a geodetic GNSS receiver and a tactical-grade inertial system), a multi-camera for panoramic image sequences, and sensor/system calibration parameters. The output is the GIS database compatible road geometry information, which contains a 3D lane model of all the lane lines visible within the camera field of view together with line type/color attributes.

The extraction of alignment data from remote sensing images has been widely explored in the past twenty years. Specific programming packages operating in the GIS environment have also been proposed in support of road element identification and selection. In an attempt to enhance the quality of road alignment data extraction, Liu et al. (2016) have recently proposed a new algorithm for the accurate extraction of the road centerline. Previously, Easa et al. (2007) and Dong et al. (2007) proposed extraction algorithms for several types of horizontal curves (simple, reverse, and spiraled).

3. SURVEY METHODOLOGIES AND STRATEGIES

In this investigation, the authors used a dedicated MM vehicle on which low-cost sensors, i.e. an integrated GPS-IMU platform and a high definition (HD) webcam, were installed (Figure 1). There is a growing interest in the use of low-cost devices to survey roads in situations where high levels of accuracy are not necessary (Higuera de Frutos and Castro, 2015). The combined use of a GNSS receiver and points derived from GIS geo-referenced aerial images facilitated the acquisition of high accuracy spatial data for comparison purposes.

Good quality aerial images in support of road alignment identification activities are available free of charge in some countries and/or regions. Frames used to identify alignment data must not be obscured by clouds or vegetation, nor affected by shadows. Sometimes, the available images may not be up-to-date, which means that what is available in the frame does not correspond to the element being surveyed. In the case of GIS data available in Vector format (e.g. shape), it is often difficult to have a perfect knowledge of the precision and accuracy with which these data were collected and processed.

Place Fig. 1 about here

This is why terrestrial methods are still of great interest and widely used in activities associated with alignment identification. The sensors are close to the object being measured, are not affected by shadows nor obscured by vegetation. MM survey systems may fail when the navigation system is affected by electromagnetic fields and high-voltage lines in the event of rain, or where the satellite signal is absent or too faint as in urban canyons. The coupling with INS sensors helps GPS receivers to continue working in such circumstances.

In this investigation, the decision to use low-cost sensors enabled the authors to investigate the potential of more affordable instrumentation in the acquisition of road alignment information. In consideration of the fact that the horizontal marking identifying the road centerline may be affected by inaccuracies due to the inevitable distortions caused by laying operations, the authors adopted different survey strategies to identify spatial data points representing the horizontal road alignment.

Firstly, it was calculated as the average point of the two trajectories followed by the MM vehicle, with data coming from a low-cost integrated GPS-IMU sensor (Table 1), and a geodetic dual frequency and dual constellation GNSS receiver (Table 2), assuming that each driving path forms a symmetrical pattern with respect to the road centerline according to Drakopoulos and Örnek (2000).

Secondly, it was extracted as the position of the central horizontal marking of the carriageway, according to the assumption made by Roh et al. (2003). It is worth noting, once again, that such a marking does not always coincide with the design and/or the as-built horizontal alignment, because of operator positioning errors.

Thirdly, the road horizontal alignment was also derived as the average line of the two carriageway edges, and fourthly as the average line of the two pavement edges. This last strategy is effective in those situations in which the marking does not exist or is of poor quality. In such cases, other identification systems based on the survey of white markings cannot be performed.

Data points representative of the alignment were extracted through the image analysis technique using a HD webcam (Table 3) implementing dedicated Matlab® algorithms (Mathworks, 2011). To do this, each frame collected by the digital video camera was geo-referenced on the basis of position data derived from GPS-IMU and GNSS sensors.

As a result, eight sequences of spatial data points were analyzed with an original algorithm developed in the Matlab® language. The characteristics of sensors employed in the investigation, and shown in Figure 1, are summarized in Table 1 (GPS-IMU), Table 2 (GNSS receiver), and Table 3 (HD webcam).

Data acquisition frequency is generally dependent on time or distance. GNSS, LiDAR and images are usually time-dependent, because the data are related to a discrete acquisition method (mirror rotation, fps, or sampling rate). In contrast, a digital map can be used to directly extract a regular dataset, which depends on the distance. By interpolation, it is also possible to extract distance-dependent datasets by means of GNSS and LiDAR measurement, although this can sometimes lead to a deterioration in the quality of the original dataset. The authors preferred to work with the original dataset, believing that the difference in data acquisition method have a negligible effect on results.

Place Table 1 about here

Place Table 2 about here

Place Table 3 about here

3.1. Centerline extraction from GNSS and GPS-IMU trajectory solutions

The vehicle trajectory data collected with GPS-IMU and GNSS sensors traveling in both directions were processed to estimate the road centerline. Two different methods were used for the estimation of the trajectories. Using the raw GNSS data, a solution with Post Processing Kinematic (PKK) techniques was reached considering a close permanent station (Leick, 2015). The trajectory collected by the integrated GPS-IMU was directly estimated adopting a loosely coupled solution, but with a lower accuracy in the absolute positioning.

During the post processing phase, for each point of the going path (p_i), a research in the return path (r_i) of all points inside a 20 m wide window (see starred points in Figure 2a) was performed. This specific window research value was selected by considering the road width. The shortest distance between each p_i and r_i was calculated (e.g., r_{i+6} in Figure 2a) by deriving the middle point (m_i). The operation was repeated for all points of the going path and the average path indicated in Figure 2b was obtained. These two datasets will be hereafter labeled as “GNSS_Traj” and “GPS-IMU_Traj” respectively.

Place Fig. 2 about here

3.2. Centerline extraction from image analysis of video sequences

During the same survey, the webcam mounted on the MM vehicle was oriented towards the front to capture the horizontal markings and the pavement edges (Piras et al., 2008). Using the collected positions and attitudes by the GPS-IMU and GNSS systems, images were then geo-referenced. The images were collected with a rate equal to 10 fps. Using the collinearity equation, the spatial position of each pixel was obtained. From an analysis of image sequences (De Agostino et al, 2010), the centerline and carriageway edge markings as well as pavement edges were used to extract several centerline solutions.

Figure 3 shows the various steps followed to convert pavement markings and edges into lines that were then converted into geo-referenced points. The extraction of such data was carried out as per the following steps:

a) image stretching to emphasize white lines, borders and other radiometric edges (Figure 3a);
b) Canny filter edge extraction on trimmed image to force feature recognition only in the road area (Figure 3b) using "edge" Matlab function;
c) Hough transform application to extract certain features (i.e. lines) which were automatically merged and classified into different layers (Figure 3c) using "hough" Matlab function;
d) decimation of extracted data through a robust, least mean squares (LMS) algorithm, with a consequent generation of a more correct and precise set of data; and
e) geo-referencing of the images, using the attitudes and positions available, performed with the plotting results saved to a dxf/dwg file (Figure 3d).

This procedure was implemented in Matlab® language with the use of some internal toolboxes devoted to image analysis (Mathworks, 2011).

Before proceeding with the image data processing, a pre-analysis of the frames was carried out with the aim of improving their quality by means of the following two steps: firstly, the grayscale conversion and, secondly, the variation of the contrast level based on the equalization histogram. These operations served to reduce computing time in proper image analysis.

The datasets assembled following the abovementioned operations will be labeled as "GNSS_CntLine", "GNSS_CigLine", "GNSS_LatLine" in the case of solutions based on the GNSS positioning system, and "GPS-IMU_CntLine" and "GPS-IMU_CigLine" in the case of solutions based on the GPS-IMU positioning system.

Place Fig. 3 about here

3.3. Centerline extraction using aerial orthophoto by means of GIS tool

To evaluate the possibility of using aerial images to get alignment information, a manual sampling process was applied to aerial images of the investigated road section (Figure 4).

A manual extraction technique was selected in order to permit a rigorous quality control check of the result obtained from the aerial images processing. In fact, while automated techniques may be more efficient with time processing related problems, they also require a subsequent quality check in order to eliminate inaccuracies, local errors, and erroneous interpretations. This quality check is generally conducted manually or by means of a series of semi-automated processes that require additional computing time and coding effort. Furthermore, automated processes are certainly more effective in cases of large scale processing, when several lines are needed to be extracted, or when the same process needs to be performed multiple times. This case study, in contrast, was perfectly suitable for a manual approach: it is relatively small (less than 3.6 km), the alignment is quite simple and in one step both the extraction and manual quality check are obtained.

Place Fig. 4 about here

The test area was covered by a photogrammetric flight in 2010, which resulted in an orthophoto with a ground sample distance (GSD) equal to 40 cm. A GIS software was used to manually determine the centerline of the case study road, maintaining a distance between points of around 10 m (Figure 4). A shape-file was produced from which a list of the nodes of the polyline generated was extracted and then imported into Matlab® to run the successive elaborations. This dataset will be hereafter labeled as "GIS_CntLine".

4. SPATIAL DATA FITTING

The authors focused their attention on the fundamental elements of the horizontal alignment, namely the circular curve centers and radii, and tangent azimuths. With a knowledge of these geometric properties, it is possible to estimate all the parameters and positions of all the alignment elements that form a road centerline: the tangent, circular arc, as well as the spirals when present. According to Bassani et al. (2016), spirals identification depends on the positioning of the adjacent tangents and circular arcs: consequently, when identified, they are

affected by low accuracy due to error propagation issues. Therefore, their estimation cannot represent a priority in any alignment identification process.

Referring to Figure 5, when tangent azimuths (ϑ_1, ϑ_2), curvature center (*C*) and radius (*R*) are identified in the horizontal plane, the curve termini (tangent to spiral – *TS*, spiral to tangent – *ST*, spiral to curve – *SC*, and curve to spiral - *CS*), and the vertex (*V*) can easily be estimated (Bassani et al., 2016).

Place Fig. 5 about here

When fitting the spatial data pertaining to a specific road element, the identification of curve termini makes it possible to distinguish between points belonging to tangents and points belonging to the circular curve. In this investigation, the operation was carried out by referring to the curvature diagram. Although the curve termini can be identified by referring to other parameters (e.g., the azimuth), the authors preferred the curvature diagram since the three basic geometric elements (tangent, circular arc and spiral transitions) are linear, while in the azimuth diagram spiral transitions are curvilinear.

To overcome any possible problems associated with the typical instabilities of the curvature diagram obtained directly from surveyed data points, the authors used a polynomial function able to fit an increasing number of spatial points. In this way, the curvature diagram tends to be more stable, smoother, and less dependent on single data positioning errors, returning a more stable result that can be further interpreted to associate spatial data with each single geometric element. Specifically, the authors adopted a local 3rd degree polynomial function that was then approximated by an osculating circular arc to obtain a local radius associated with each surveyed point.

Accordingly, the curve termini were identified by grouping the series of points that presented a relatively constant curvature. This operation was carried out by analyzing the curvature diagram obtained for each dataset, like the diagram shown in Figure 6 and obtained on data coming from the interpretation of aerial orthophotos.

Place Fig. 6 about here

The diagram reports the results obtained with an increasing number of points (from 5 to 21) fitted by the 3rd degree polynomial function. Matching the curvature obtained from each dataset with the information coming from the as-built project, the spatial data points have been grouped and assigned to one of the three relevant elements (tangent, spiral, circular arc).

Once the spatial data points have been grouped, the geometric characteristics of the two elements (tangent and circular arc) can be estimated. The basic equation for the circular arcs in the (*x*,*y*) plane is:

$$x^2 + y^2 + ax + by + c = 0 \qquad \text{eq. 1}$$

where *a*, *b* and *c* are the parameters that fully define its position and characteristics. In fact, the radius (*R*) and curve center coordinates (x_c, y_c) are derived from the following equations:

$$x_c = -\frac{a}{2} \qquad \text{eq. 2}$$

$$y_c = -\frac{b}{2} \qquad \text{eq. 3}$$

$$R = \sqrt[2]{{x_c}^2 + {y_c}^2 - c} \qquad \text{eq. 4}$$

When a number N of points discretizes a circular arc, starting from eq. 1 the system of N equations:

$${x_i}^2 + {y_i}^2 + \mathrm{a}x_i + \mathrm{b}y_i + \mathrm{c} = \mathrm{v}_i \qquad \text{eq. 5}$$

can be solved by means of statistical and/or numerical methods to calculate *a*, *b* and c (Bassani et al., 2016). In eq. 1, the term v_i represents the possible error between the observed value and the fitted (or residual) value.

The most common statistical method using a rigorous and accurate approach to solve a system of equations is the Least Squares (LS) method. This fitting method is suggested when the system has a good redundancy and when the number of gross errors (or outliers) is limited. By separating known terms (x_i, y_i) from unknown terms (*a, b, c*), eq. 1 becomes similar to the generic matrix-vector notation to which LS methods are generally applicable:

$$Ak - l_0 = v \qquad \text{eq. 6}$$

where:

$$A = \begin{bmatrix} x_1 & y_1 & 1 \\ x_2 & y_2 & 1 \\ x_3 & y_3 & 1 \\ \cdots & \cdots & \cdots \\ x_n & y_n & 1 \end{bmatrix} \quad , k = \begin{bmatrix} a \\ b \\ c \end{bmatrix} \quad , l_0 = \begin{bmatrix} -x_1^2 - y_1^2 \\ -x_2^2 - y_2^2 \\ -x_3^2 - y_3^2 \\ \cdots \\ -x_n^2 - y_n^2 \end{bmatrix}$$

in which A is the design matrix, which represents the matrix of the coefficients of the unknown parameters, k is the vector of unknown terms, and l_0 is the vector of known terms. The solution to k is (Cina, 2007):

$$\hat{k} = (A^T A)^{-1} A^T A l_0 \qquad \text{eq. 7}$$

Once (a, b, c) are calculated, (x_c, y_c) and R can also be estimated. The same process can be performed on tangents, the basic equation for which is:

$$y = mk' + q \qquad \text{eq. 8}$$

where m is the angular coefficient indicating their direction, and q is the intercept with the y axis. The LS generic matrix-vector notation assumes the following form:

$$A = \begin{bmatrix} x_1 & 1 \\ x_2 & 1 \\ x_3 & 1 \\ \cdots & \cdots \\ x_n & 1 \end{bmatrix}$$

$$k' = \begin{bmatrix} m \\ q \end{bmatrix}$$

$$l_0 = \begin{bmatrix} y_1 \\ y_2 \\ y_3 \\ \cdots \\ y_n \end{bmatrix}$$

Although this approach provides an accurate solution, it can be affected by gross errors. It is, therefore, fundamental to include the use of some statistical tests devoted to outlier detection or data analysis (Baarda, 1967; 1968).

Huber (2011) classifies the methods into the following three groups: (a) outliers in the y-direction: the most common technique being the Huber estimator; (b) moderate percentage

of outliers in the coordinate space (leverage points); Mallows and Schweppe being the most popular estimator; and (c) outliers in both the x and y directions with high frequency; in this case high breakdown estimators are used.

In all these methods, the aim is to use a robust estimator with a high breakdown point, which is the minimum fraction of outlying data that can cause an estimate to diverge arbitrarily from the true estimate. The object function of the Least Median of Squares (LMS) is to minimize the median value of the squared residuals. The LMS estimate is equivalent to linear transformations of the draw matrix and it has a breakdown point equal to 50%. In this investigation, the Huber estimator was adopted in the Matlab® routine (Mathworks, 2011), where the specific statistic toolbox denominated "robustfit" was used. In this toolbox, the value of the weight function was set equal to 1.345.

The computing process can be summarized by the flow chart in Figure 7, independently of the fitting algorithm implemented (least squares or robust estimator). The process starts loading the first available centerline solution.

Place Fig. 7 about here

A couple of checks are performed: (a) on the element type, since fitting is possible only on tangents and circular curves; and (b) on the number of points that constitute each element, since the fitting process requires three points for tangents and four for circular curves.

If both tests are positive, the fitting procedure can proceed and the matrix *A* and vector l_0 are prepared; in the case of an insufficient number of points, an error message is stored. When the fitting is complete, the algorithm switches to the next centerline solution.

5. CASE STUDY

Figure 8 shows the twenty-five elements of the horizontal alignment used as a case study. The segment lies between two roundabouts located along the National Route n. 23 in the suburbs of Turin (Italy). The base value of the circular arc adopted by the designer was equal to 550 m, which was selected for curves 5, 9, 13, 17, and 21.

Table 4 provides as-built information consisting of the number and type of horizontal elements, their length, chainage of curve termini, the radius, the center of curvature, and tangent direction (angular coefficients). It should be noted that the authors do not have specific information on the methodology (i.e., level of accuracy) adopted by the road agency in the definition of the as-built horizontal alignment.

Place Fig. 8 about here

To simplify data interpretation, a local reference system was adopted rather than the initial UTM-WGS84 reference system. Hence, each single coordinate has been reduced by an amount equal to 386887.4198 m in the East component, and 4979559.0127 m in the North component.

The centerline solutions investigated are summarized in Table 5. The second column gives the designation to be adopted in subsequent tables and figures, then there is the position reference adopted (GIS, GNSS or GPS-IMU), followed by the accuracy, the number of geo-referenced points in which the solution was discretized, and, finally, the average spacing between points. To compare fitted results with the most readily available correct reference values, a discretization of the as-built centerline was carried out with a spacing of 0.5 m. The same fitting algorithm was then used to back-calculate both survey-based and as-built-based horizontal alignment solutions. Figure 9 provides a local representation of data points reported in the UTM-WGS84 reference system.

Place Table 4 about here

Place Table 5 about here

Place Fig. 9 about here

6. RESULTS AND DISCUSSION

Figure 10 provides a graphic overview of the fitting results. The graphs in the first column correspond to the fitting of curves radii, where each bar represents a combination of the horizontal alignment solution and fitting algorithm adopted (least squares – LS, and Huber - HB) and described in Section 3. The graphs in the second column relate to tangents. The dashed lines represent the expected values derived from the fitting of the as-built data with points distanced 0.5 m apart.

Figure 10 clearly illustrates the satisfactory nature of the results obtained with GIS-based track solutions, which is attributable to the fact that aerial images were directly interpreted without any other elaboration that could introduce and/or propagate errors, notwithstanding that the nominal accuracy reported in Table 1 is affected by GSD.

Place Fig. 10 about here

Although spatial data collected using MM techniques lead to good results under certain conditions, they generally suffer from error propagation effects. Data derived from the average of extracted GPS-IMU or GNSS based trajectories are more accurate than those obtained from the analysis of images captured through a HD webcam. In the former, trajectories are directly obtained from an onboard positioning system, while in the latter, the data sets are extracted from the images captured by webcams. This means that the error inside the image extraction process is combined with the inaccuracies of the positioning system. Nevertheless, fitting results are generally good in the case of curve #17, which is the longest curve of the alignment.

According to Bassani et al. (2016), this is not surprising, since in the identification of circular arcs, the quality of the results depends on the geometric characteristics of the elements that have to be estimated, and in particular on the length of the curve and the radius magnitude. Furthermore, it also depends on the level of accuracy used to survey data points, and the fitting method used. As expected, Huber estimation is more efficient in the case of outliers, whereas fitting solutions obtained from the LS algorithm generally lead to poorer results, as confirmed by data reported in Figure 10. However, the difference between the two algorithms appears minimal in most cases, and this is certainly due to the limited presence of outliers in the case of some solutions. Table 6 reports the difference between the as-built fitted radii and those extracted with the least squares (LS) and Huber techniques (HB). The error is expressed as a percentage of the as-built corresponding value.

Values are only available for main curves (#5, #9, #13, #17, #21 and #25), while the first curve (#1) was excluded since the MM vehicle trajectories were heavily influenced by the presence of the roundabout. It is worth noting that the solution derived from the as-built changes in accordance with differences in the spacing adopted. Missed value (n.a.) indicates that the fitting could not be performed due to an insufficient number of data points (a minimum number of points is necessary to provide some redundancy to the fitting process).

Table 7 displays the horizontal distances between fitted and as-built curvature centers. This parameter is effective when there is a need to compare the distance between two points on the (x,y) plane: the shorter the distance, the better the fitting. Similar conclusions to those corresponding to curve radii can be drawn: better results were obtained in the case of curve #17, which is the longest curve in the analyzed road section, and HB solutions are more accurate than LS ones.

Finally, Table 8 shows the results for tangent directions. Tangent characterization is the easiest recognition process in terms of stability and accuracy of results. Independently of the source of data, the result is for the most part excellent with only 3% of the target direction values affected by an error. The fitting algorithms adopted overcome any inaccuracies in point positioning or possible local defects with ease. The quality of extracted tangent directions is high enough to perform a geometrical reconstruction of the main polygonal obtainable from the extension of tangents.

Place Table 6 about here

Place Table 7 about here

Place Table 8 about here

Once again, from Table 6, 7 and 8 it is evident that the estimation of the circular arc is the most challenging task, and that it is sensitive to factors like the accuracy of the data collection method and, most of all, the geometry of the curve. In fact, when curves are short in length (i.e., curve #5, 9, 13 and 21), problems in the fitting estimation may occur (Bassani et al., 2016). Thus, the variability in the results cannot be accounted for solely by the number of points, the positioning accuracy or sampling frequency.

7. CONCLUSIONS

Too often, alignment data for existing roads are unavailable, in an unsuitable format, and/or not updated. Accordingly, various geospatial data collection methodologies, techniques, and identification methods have been proposed to support road engineers in activities for which a knowledge of road alignment is fundamental.

This work deals with such aspects, and seeks to make a contribution by comparing different methodologies for the identification of the horizontal alignment of existing roads. Such comparisons might be useful for survey practitioners who have to make a choice between different techniques while subject to both budgetary and desired accuracy level constraints. As is evident from Table 9, certain techniques often present advantages in terms of acquisition time, but generally require significant economic investment. Low-cost sensors and methodology validation and comparison are important factors to consider in the selection process.

The case study results provide useful information regarding the possibility of extracting alignment information such as curve radii and centers, and tangent orientations. Regarding the survey methodologies investigated here:

a) the data obtained by integrated GPS-IMU low-cost sensors are comparable to those from high-cost GNSS receivers in the case of trajectory-based solutions from a relative accuracy point of view;
b) the data extracted using the geo-referenced images, as per the methodology described in Section 3.2, are less accurate than those gathered with other techniques, because the poor accuracy of the geo-referencing causes error propagation in the pixel position and then in the extracted road elements;
c) the alignment identification carried out on aerial images available on GIS led to good results, since the methodology is not affected by error propagation issues.

Regarding the survey strategies investigated here:

a) recourse to the survey of the two pavement edges to derive the road alignment as the average line may lead to significant inaccuracies both in the estimation of the curve radius (i.e., curves #5, #9, #13, #21) and in the tangent azimuth (i.e., tangents #3 and #11); pavement edge lines may result irregular due to the presence of vegetation and other roadside elements such as traffic barriers;
b) results obtained when the data points used to back-calculate the horizontal alignment derive from the vehicle trajectories appear to be satisfactory; in the case study investigated here, the range in error when estimating the radius was between +25.6 and – 21.2%, while larger values were obtained with other strategies.

The paper also confirms the results obtained in a recent paper by the authors (Bassani et al., 2016). In particular, when the data points describing the circular curve are sufficient in number (or when the curve has a sufficient length), the LS and HB fitting methods exhibit similar behaviors. When large outliers affect the data, robust methods (i.e., HB) are more effective in the identification of the center of curvature and the radius value. Finally, the results highlight that when only a small number of points are available with respect to radius size, or when the curve is too short, the methods employed here are not effective and fail in the identification of the radius and center of curvature.

As demonstrated in this study, geomatics techniques are appropriate for the collection of spatial data to identify the horizontal alignment of highways. Moreover, each technique

attains a different level of accuracy and performance in terms of acquisition and processing time, as well as device, acquisition and data treatment costs. Sometimes, the time and cost required to carry out surveys are not consistent with the investigation aims and budget available.

Table 9 compares such information for the techniques employed in this investigation. One advantage of using orthophotos is the high productivity in terms of the area covered with respect to time. Furthermore, orthophoto and aerial images are usually open data that may be accessible to the public, in which case, the cost is very low. The method would, however, be less effective in small or restricted areas, and available images may also be out of date. In such cases, the use of images gathered by drones could represent a fast and cheap alternative, with a limited cost both for the system and data acquisition. However, the use of the system depends on national regulations regarding the operation of unmanned flight systems over roads and built-up areas.

Good quality aerial images in support of road alignment identification activities are only available free of charge in some countries and/or regions. To ensure good quality, frames should not be obscured by clouds, vegetation, nor shadows. Furthermore, the available images may not be up-to-date, which means that what is available in the frame may not correspond to the actual road section being surveyed.

The MM with low cost GPS-IMU sensors is recommended for investigations over short-to-middle distances and when extremely accurate solutions for the road alignment are not required. MM methods still retain great potential because the sensors are close to the object being measured, they are not affected by shadows and they are not obscured by vegetation. Terrestrial survey systems only fail in the event of inaccuracies with the navigation system, which can be affected by electromagnetic fields and high-voltage lines in wet conditions, or where the satellite signal is absent or too faint due to the presence of urban canyons or high noise levels. Although the financial outlay is limited due to the employment of low-cost sensors, the calibration and processing tasks require a long time.

Finally, MM systems operating with GNSS are used when there is the need for a highly accurate solution. It is widely used in the formation of road cadastral, and supports high performance surveys in terms of km acquired/€, therefore it is not ideal for short distances. This solution, which incorporates high-cost sensors, is the de-facto commercial standard.

Place Table 9 about here

ACKNOWLEDGEMENTS

The research presented in the paper refers to part of the activities carried out in the Pro-Vision Project, which was funded by the Regione Piemonte (F.E.S.R. 2007/2013).

REFERENCES

Ai, C., Tsai, Y., 2014. Automatic Horizontal Curve Identification and Measurement Method Using GPS Data. J. of Transp. Eng. 141(2), 04014078.

Baarda, W., 1966. Statistical concepts in geodesy. Netherlands Geodetic Commission, Publications on Geodesy, 2(4), 74.

Baarda, W., 1968. A testing procedure for use in geodetic network. Netherlands Geodetic Commission, Publications on Geodesy, 2(5), 97.

Bassani, M., Lingua, A., Piras, M., De Agostino, M., Marinelli, G., Petrini, G., 2012. Alignment data collection of highways using mobile mapping and image analysis techniques. Proceedings Transportation Research Board Annual Meeting, Washington D.C, 12-0312.

Bassani, M., Marinelli, G., Piras, M., 2016. Identification of Horizontal Circular Arc from Spatial Data Sources. J. Surv. Eng. 142(4), 04016013.

Benedetto, C., 2000. La Sicurezza Stradale. Il Contributo della Ricerca Scientifica. Rome, Italy (in Italian).

Beauvais, M., Lakshmanan, S., 2000. Clark: A heterogeneous sensor fusion method for finding lanes and obstacles. Image and Vis. Comp. 18(5), 397-413.

Castro, M., Iglesias, L., Rodríguez-Solano, R., Sánchez, J. A., 2006. Geometric modelling of highways using global positioning system (GPS) data and spline approximation. Transp. Res. Part C: Emerg. Technol. 14(4), 233-243.

Cheng, W., Hassan, T., El-Sheimy, N., Lavigne, M., 2008. Automatic road vector extraction for mobile mapping systems. The Int. Arch. of the Photog., Rem. Sens. and Spat. Info. Sci. 37(Part B3b), 515-521.

Choi, S., Sung, J., 2006. Data generalization algorithm for the extraction of road horizontal alignment design elements using the GPS/INS data. Advances in Hybrid Information Technology (51-62). Springer Berlin Heidelberg.

Choi, S. Y., Lee, J. M., 2006. Applications of moving windows technique to autonomous vehicle navigation. Image and Vis. Comp. 24(2), 120-130.

Cina, A., 2007. Trattamento delle misure topografiche. Torino-Celid (in Italian).

Crisman, B., Robba, A., 2004. Safety Evaluation: Practical Use Of Collected-Data Vehicle To Obtain Geometric Information Of Existing Roadways. 2nd SIIV International Congress, 1, Florence, Italy.

de Frutos, S. H., Castro, M., 2014. Using smartphones as a very low-cost tool for road inventories. Transp. Res. Part C: Emerg. Technol. 38, 136-145.

De Agostino, M., Lingua, A., Marenchino, D., Nex, F., Piras, M. 2011. GIMPHI: a new integration approach for early impact assessment. Appl. Geom. 3(4), 241-249.

Dong, H., Easa, S. M., & Li, J., 2007. Approximate extraction of spiralled horizontal curves from satellite imagery. J. Surv. Eng. 133(1), 36-40.

Drakopoulos, A., Örnek, E., 2000. Use of vehicle-collected data to calculate existing roadway geometry. J. Transp. Eng. 126(2), 154-160.

Easa, S. M., Dong, H. M., Li, J., 2005. Use of satellite imagery for establishing road horizontal alignments. J. Surv. Eng. 133(1), 29–35.

Findley, D. J., Cunningham, C. M., Hummer, J. E., 2011. Comparison of mobile and manual data collection for roadway components. Transp. Res. Part C: Emerg. Technol. 19(3), 521-540.

Freeman, W. T., Adelson, E. H., 1991. The design and use of steerable filters. IEEE T. Pattern Anal. 9, 891-906.

Gruen, A., Li, H., 1995. Road extraction from aerial and satellite images by dynamic programming. ISPRS J Photogramm. 50(4), 11-20.

Guan, H., Li, J., Yu, Y., Wang, C., Chapman, M., Yang, B. 2014. Using mobile laser scanning data for automated extraction of road markings. ISPRS J Photogramm. 87, 93-107.

Hu, Z., Uchimura, K., 1999. Action-based road horizontal shape recognition. SBA Controle and Automaçao 10(2), 83-88.

Huber, P. J., 2011. Robust statistics (pp. 1248-1251). Springer Berlin Heidelberg.

Harkey, D., Yi, C., Feaganes, J., 2004. Evaluation and validation of automated in-vehicle data collection system for developing roadway alignments. Transport. Res. Rec. 1897, 164-172.

Higuera de Frutos, S. H., Castro, M. (2014). Using smartphones as a very low-cost tool for road inventories. Transp. Res. Part C: Emerg. Technol. 38, 136-145.

Holgado-Barco, A., González-Aguilera, D., Arias-Sanchez, P., Martinez-Sanchez, J., 2015. Semiautomatic extraction of road horizontal alignment from a mobile LiDAR system. Comp.-Aid. Civil and Infr. Eng. 30(3), 217-228.

Hough, P. V., 1959. Machine analysis of bubble chamber pictures. International Conference on High Energy Accelerators and Instrumentation (Vol. 73).

Imran, M., Hassan, Y., Patterson, D., 2006. GPS–GIS-Based Procedure for Tracking Vehicle Path on Horizontal Alignments. Comp.-Aid. Civil and Infr. Eng. 21(5), 383-394.

Ishikawa, S., Kuwamoto, H., Ozawa, S., 1988. Visual navigation of an autonomous vehicle using white line recognition. IEEE T. Pattern Anal. 10(5), 743-749.

Jochem, T. M., Pomerleau, D. A., Thorpe, C. E., 1993. MANIAC: A next generation neurally based autonomous road follower. Proceedings of the International Conference on Intelligent Autonomous Systems: IAS-3. Pittsburgh, Pennsylvania, USA.

Leick, A., Rapoport, L., Tatarnikov, D. (2015). GPS Satellite Surveying. John Wiley & Sons.

Li, Q., Zheng, N., Cheng, H., 2004. Springrobot: A prototype autonomous vehicle and its algorithms for lane detection. IEEE T. Int. Transp. Syst. 5(4), 300-308.

Li, Z., Chitturi, M., Bill, A., Noyce, D., 2012. Automated identification and extraction of horizontal curve information from geographic information system roadway maps. Transport. Res. Rec. 2291, 80-92.

Lin, Y., Hyyppa, J., & Jaakkola, A., 2011. Mini-UAV-borne LIDAR for fine-scale mapping. IEEE Geosci. Remote S. 8(3), 426-430.

Liu, R., Miao, Q., Huang, B., Song, J., & Debayle, J., 2016. Improved road centerlines extraction in high-resolution remote sensing images using shear transform, directional morphological filtering and enhanced broken lines connection. J. of Vis. Comm. and Image Repr. 40, 300-311.

López, A., Serrat, J., Cañero, C., Lumbreras, F., Graf, T., 2010. Robust lane markings detection and road geometry computation. Int. J. Auto. Tech. Kor. 11(3), 395-407.

MathWorks, 2011. MATLAB User Manual. Natik, Massachusetts.

McCall, J. C., Trivedi, M. M., 2004. An integrated, robust approach to lane marking detection and lane tracking. IEEE Int. Veh. Sym., 533-537.

Piras, M., Cina, A., Lingua, A. (2008, May). Low cost mobile mapping systems: an Italian experience. IEEE/ION Position, Location and Navigation Symposium, 1033-1045.

Roncella, R., Forlani, G., 2006. Automatic lane parameters extraction in Mobile Mapping sequences. Proceedings of the ISPRS, Commission V Symposium.

Roh, T. H., Seo, D. J., Lee, J. C., 2003. An accuracy analysis for horizontal alignment of road by the kinematic GPS/GLONASS combination. KSCE J. Civ. Eng. 7(1), 73-79.

Tai, J. C., Tseng, S. T., Lin, C. P., Song, K. T., 2004. Real-time image tracking for automatic traffic monitoring and enforcement applications. Image and Vis. Comp. 22(6), 485-501.

Tao, C. V., Chapman, M. A., Chaplin, B. A., 2001. Automated processing of mobile mapping image sequences. ISPRS J Photogramm. 55(5), 330-346.

Tarel, J. P., Ieng, X. S., Charbonnier, P., 2007. Accurate and robust image alignment for road profile reconstruction. IEEE International Conference on Image Processing, 2007. ICIP 2007 (Vol. 5, pp. V-365).

Toth, C., Grejner-Brzezinska, D., 2004. Redefining the Paradigm of Modern Mobile Mapping. Photogramm. Eng. Rem. S. 70(6), 685-694.

Tsai, Y. J., Wu, J., Wang, Z., Hu, Z., 2010. Horizontal roadway curvature computation algorithm using vision technology. Comp.- Aid. Civil and Infr. Eng. 25(2), 78-88.

LIST OF FIGURE

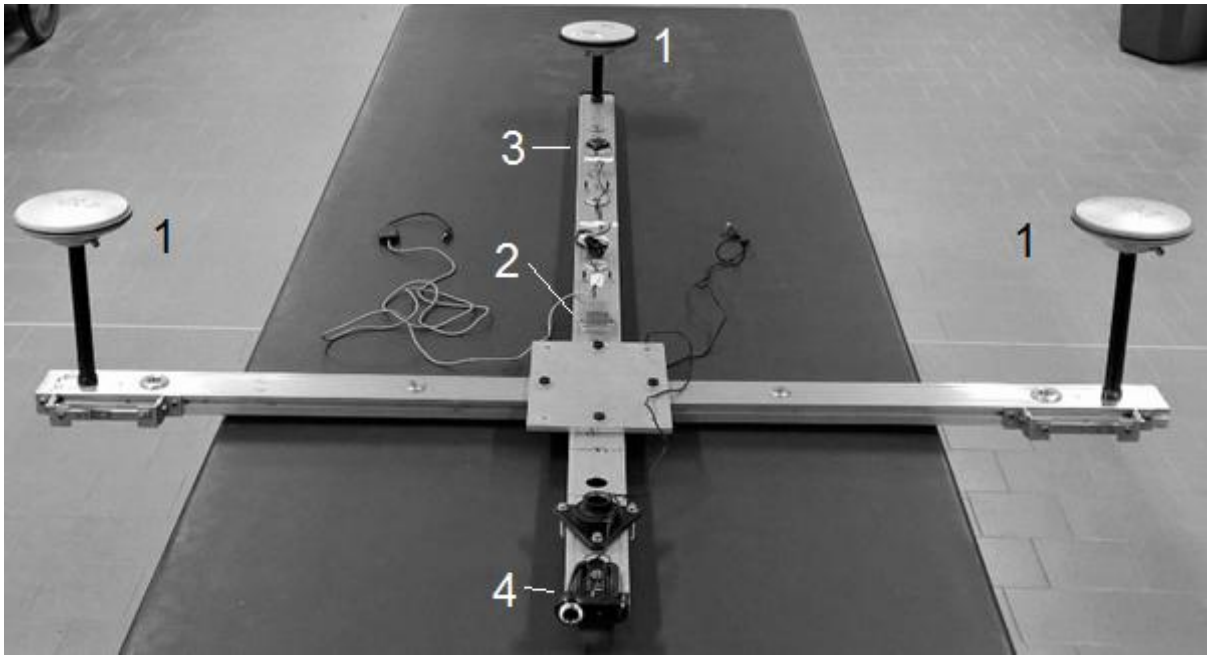

Fig. 1. MM system with on-board sensors (1 = Geodetic GNSS antenna connected to GNSS receiver Leica 1200, 2 = GPS-IMU platform, 3 = antenna patch connected to the GPS-IMU, 4 = HD webcam).

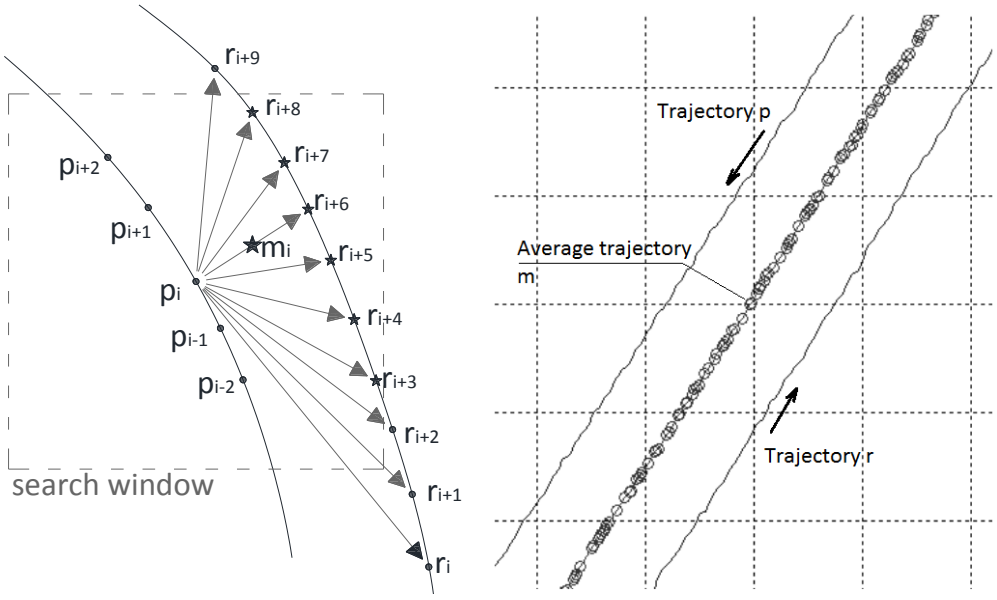

(a) (b)

Fig. 2. Average trajectory process/result example. (a) Research of closest point, and (b) average line between the two trajectories along a tangent section.

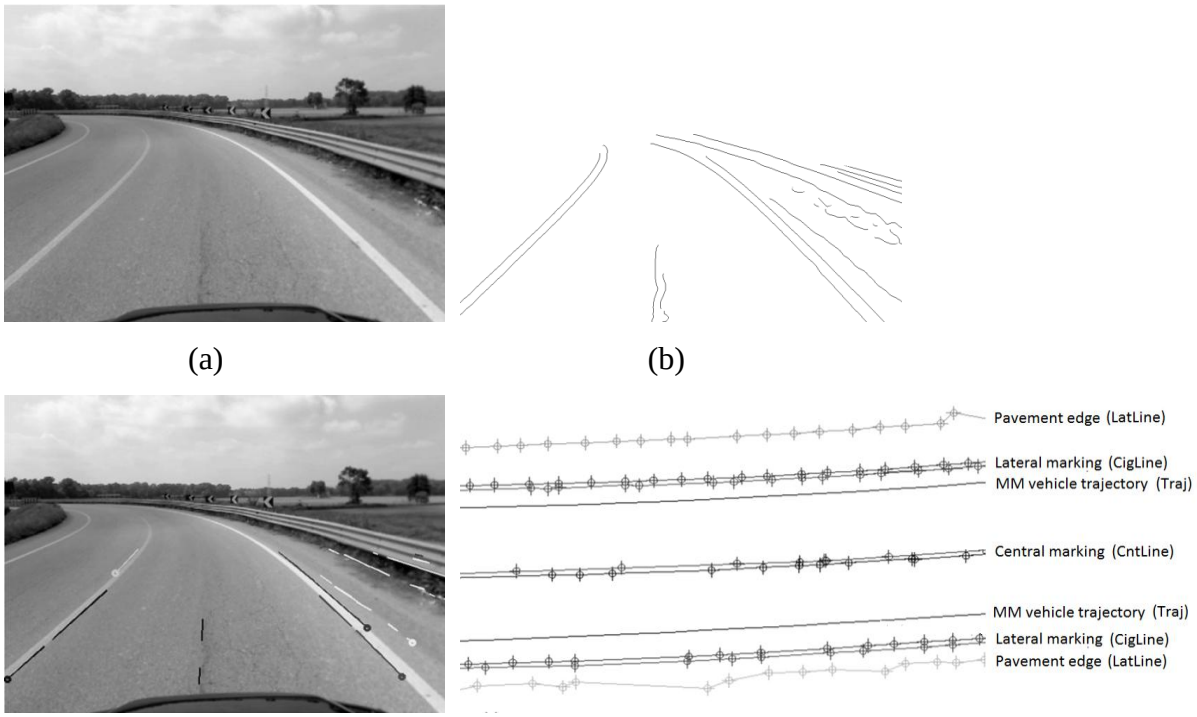

Fig. 3. Image analysis process main steps. (a) RGB original image, (b) edges extraction with Canny filter, (c) features recognition with Hough transform, and (d) features geo-referencing.

Fig. 4. Points of the centerline extracted by orthophoto images in GIS environment.

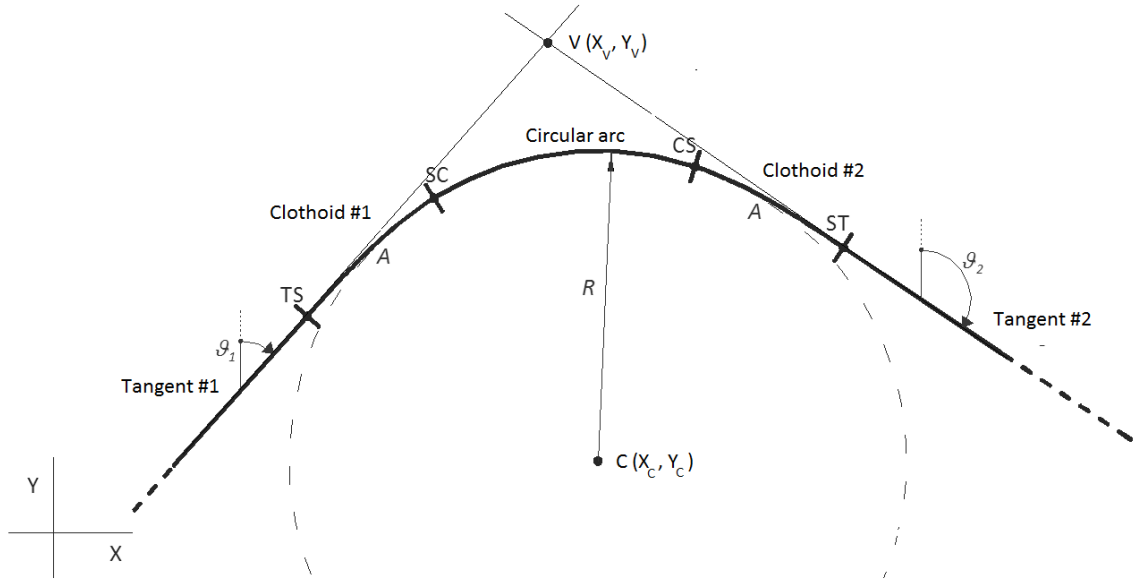

Fig. 5. Combined curve with spirals and circular arc.

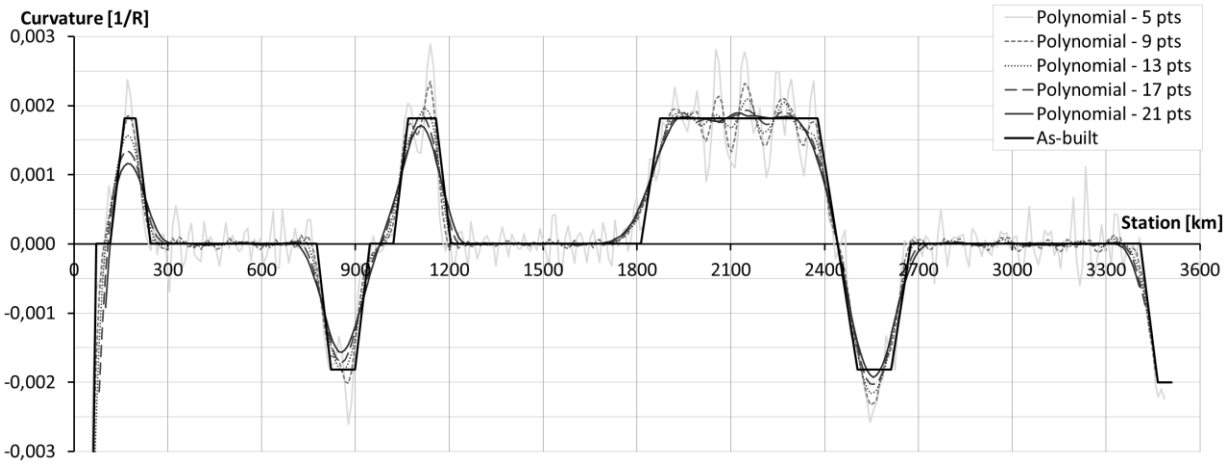

Fig. 6. GIS_CntLine local curvature graph with 3rd degree polynomial function and various fitting window widths.

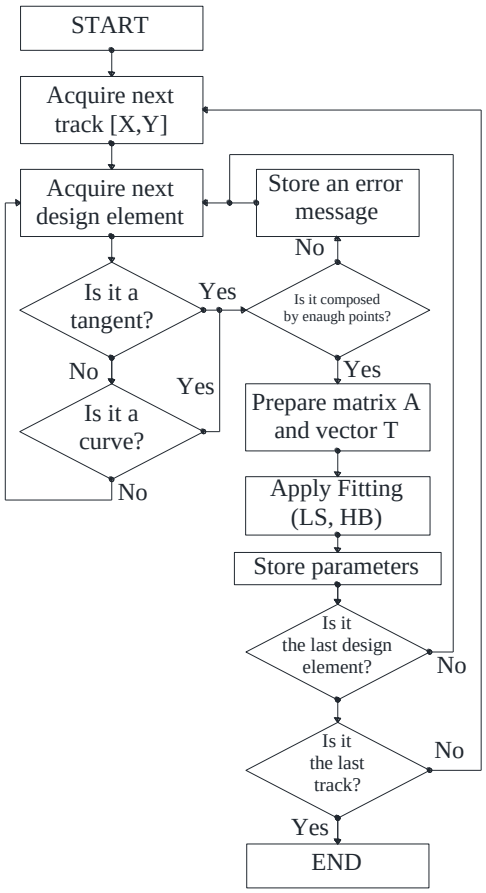

Fig. 7. Flow chart of the fitting process.

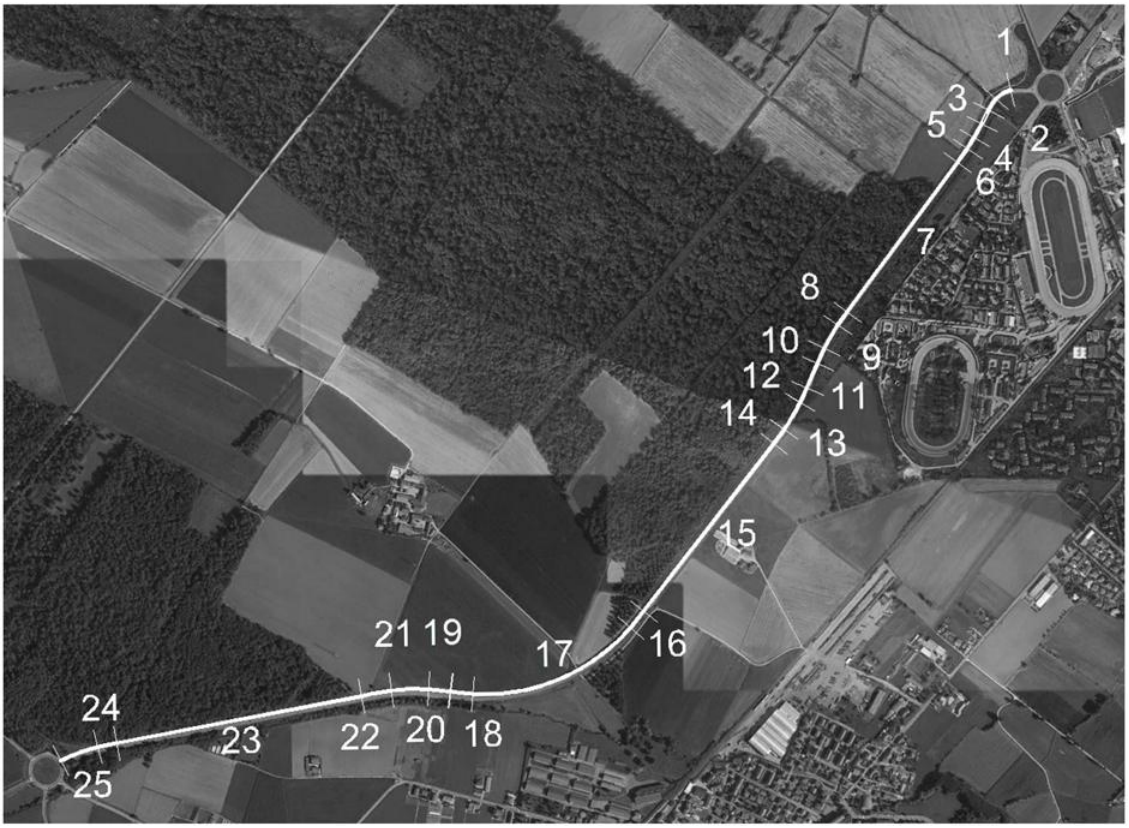

Fig. 8. Horizontal alignment of the case study.

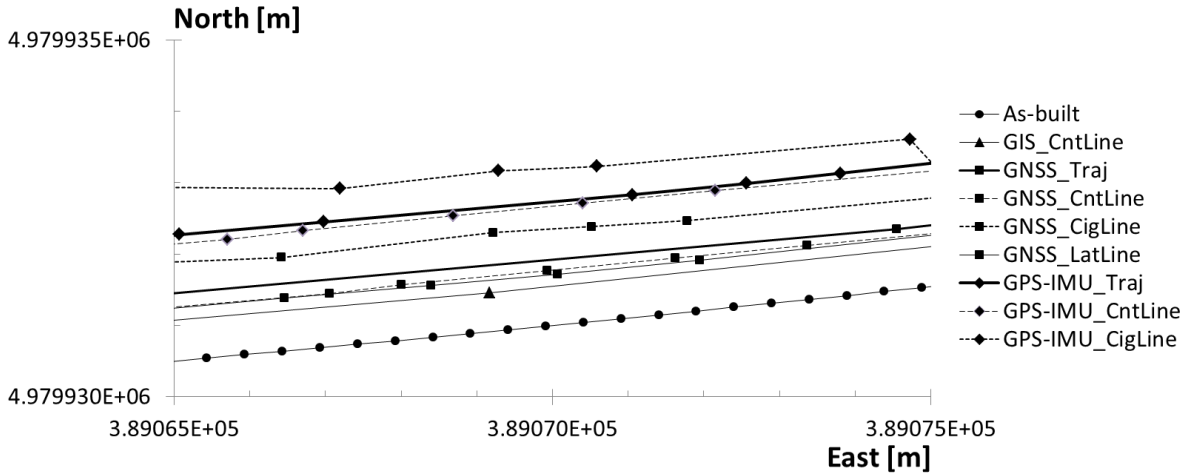

Fig. 9. Zoom on the eight centerline solutions and the as-built horizontal alignment (UTM-WGS84 reference system).

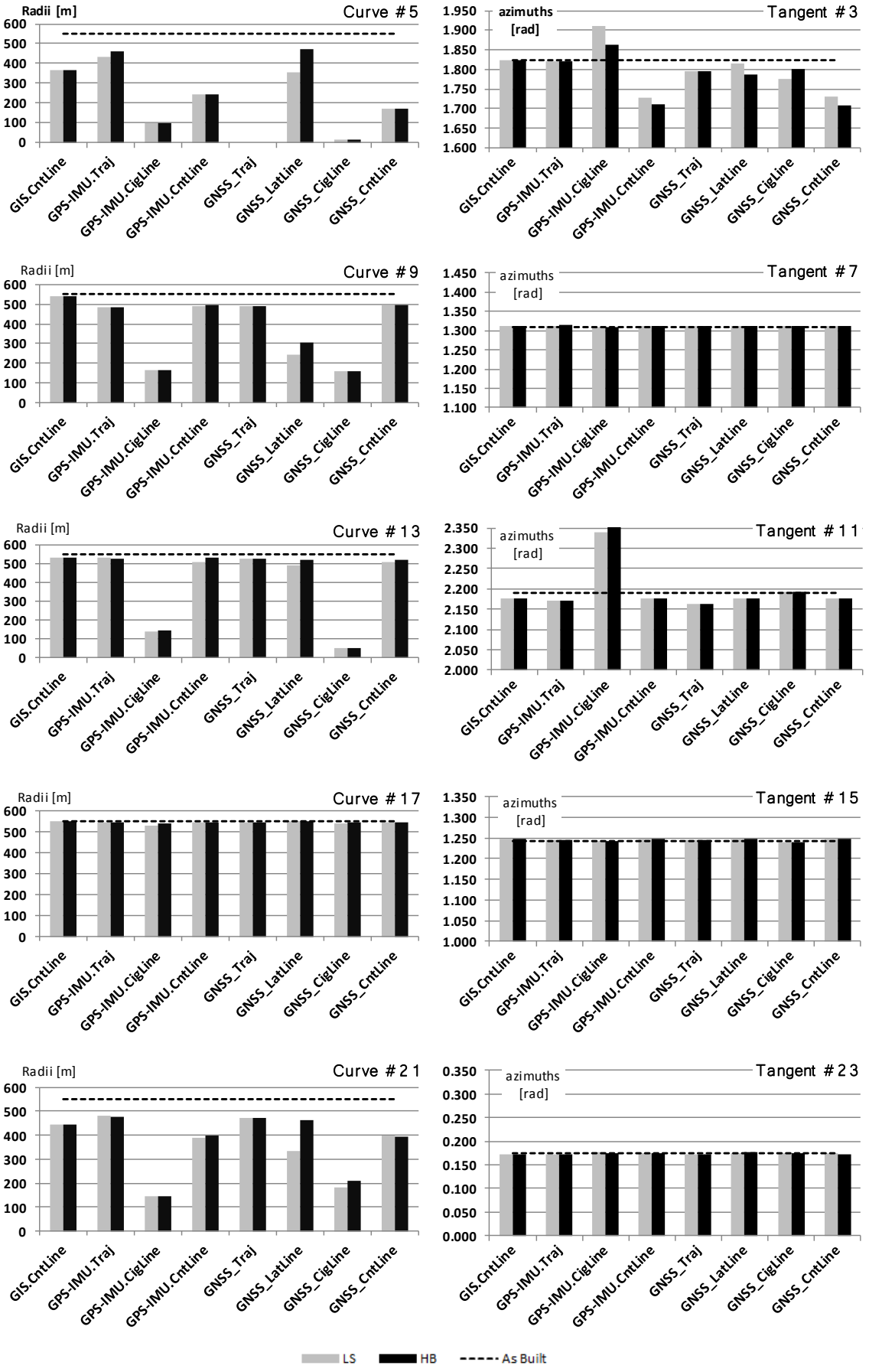

Fig. 10. Synthesis of fitting results.

LIST OF TABLES

Table 1. GPS-IMU specifications.

Cost, k€	1
Angular Rate:	
Range Roll, Pitch, Yaw (°/s)	± 300
Bias: Roll, Pitch (°/s)	± 0.5
Bias: Yaw (°/s)	± 1.0
Resolution (°)	0.05
Acceleration:	
Range X/Y/Z, m/s^2	± 50
Bias: X/Y/Z, m/s^2	± 0.02
Resolution, m/s^2	0.0098
Update Rate, Hz	512
Internal GPS:	
Raw Measurements	L1 frequency, C/A code
No. Channels	50
Max. update rate, Hz	4
Operating temperature, °C	–40 to 85

Table 2. GNSS receiver specifications.

Cost, k€	15
Constellation	GPS, GLONASS, GALILEO, WAAS, COMPASS
Frequencies	L1, L2, L5
Weight, g	~ 600
Power consumption, W	4.6
External Antenna	Yes
RTK	Yes
Positioning, cm	1-3
Real time, mm	1-10

Table 3. HD webcam specifications.

Cost, k€	0.15
Resolution	960 x 720
Frame per second	8
Camera lens	Carl Zeiss optics with autofocus
Image format	jpeg

Table 4. As- built road composition.

#	Element type	Length [m]	Chainage [m]	Radius [m]	Spiral scale parameter [m]	Tangent azimuth [rad]	Circular arc center in a local reference system	
							X_c [m]	Y_c [m]
1	Circular curve	49.28	0.00	80			3662.959	1987.614
2	Clothoid	37.81	49.28		55.00			
3	Tangent	43.71	87.09			1.824		
4	Clothoid	46.55	130.80		160.00			
5	Circular curve	36.71	177.35	550			3068.487	2215.690
6	Clothoid	46.55	214.06		160.00			
7	Tangent	531.67	260.60			1.309		
8	Clothoid	46.55	792.27		160.00			
9	Circular curve	76.63	838.82	550			3591.773	1088.203
10	Clothoid	46.55	915.45		160.00			
11	Tangent	75.23	961.99			2.189		
12	Clothoid	46.55	1037.22		160.00			
13	Circular curve	90.67	1083.77	550			2540.317	1434.600
14	Clothoid	46.55	1174.44		160.00			
15	Tangent	607.43	1220.99			1.243		
16	Clothoid	62.23	1828.42		185.00			
17	Circular curve	504.48	1890.64	550			2125.402	919.006
18	Clothoid	62.23	2395.12		185.00			
19	Tangent	2.23	2457.35			-0.138		
20	Clothoid	62.23	2459.58		185.00			
21	Circular curve	105.59	2521.81	550			1911.239	-162.465
22	Clothoid	62.23	2627.40		185.00			
23	Tangent	733.08	2689.62			0.174		
24	Clothoid	57.80	3422.70		170.00			
25	Circular curve	111.66	3480.50	500			1121.337	-249.350
		Total:	3592.16					

Table 5. Centerline solutions overview.

# Centerline solutions	Designation	Reference positioning system	Accuracy	# points	Spacing [m]
1 Centerline manual sampling	GIS_CntLine	GIS	~ 0.5 m	349	10.08
2 Vehicle trajectory average (RT)	GNSS_Traj	GNSS	2 ÷ 4 cm	240	14.71
3 Centerline average (RT)	GNSS_CntLine	GNSS	1 cm ÷ 1 m (*)	1397	2.52
4 Roadside average (RT)	GNSS_CigLine	GNSS	1 cm ÷ 1 m (*)	2002	2.08
5 Lateral line average (RT)	GNSS_LatLine	GNSS	1 cm ÷ 1 m (*)	1847	1.98
6 Vehicle trajectory average (RT)	GPS-IMU_Traj	GPS-IMU	~ 2.5 m	2129	1.67
7 Centerline average (RT)	GPS-IMU_CntLine	GPS-IMU	1 cm ÷ 1 m (*)	1338	2.64
8 Roadside average (RT)	GPS-IMU_CigLine	GPS-IMU	1 cm ÷ 1 m (*)	2132	2.07

RT= with round trip

(*) the accuracy depends on the distance between MMS and the object

Table 6. Percentage errors in the estimation of radii.

Element #		GIS CntLine	GPS-IMU Traj	GPS-IMU _CigLine	GPS-IMU _CntLine	GNSS Traj	GNSS LatLine	GNSS CigLine	GNSS CntLine
#5	LS	-33,2 %	-21,2 %	-82,1 %	-56,1 %	n.a.	-35,6 %	-96,9 %	-68,9 %
	HB	-33,2 %	-16,5 %	-82,1 %	-56,0 %	n.a.	-14,7 %	-96,9 %	-68,9 %
#9	LS	-1,4 %	-11,5 %	-69,5 %	-10,7 %	-11,2 %	-55,9 %	-70,8 %	-10,0 %
	HB	-1,4 %	-11,5 %	-69,6 %	-10,0 %	-11,2 %	-44,8 %	-70,5 %	-10,3 %
#13	LS	-3,8 %	-3,2 %	-74,9 %	-7,6 %	-4,6 %	-10,8 %	-90,3 %	-7,2 %
	HB	-3,8 %	-4,4 %	-73,9 %	-3,2 %	-4,6 %	-5,4 %	-90,9 %	-5,9 %
#17	LS	-0,09 %	-1,1 %	-4,0 %	-1,3 %	-0,6 %	0,1 %	-2,2 %	-0,8 %
	HB	-0,06 %	-1,1 %	-2,3 %	-1,1 %	-0,6 %	-0,3 %	-1,3 %	-0,7 %
#21	LS	-19,4 %	-12,8 %	-73,3 %	-28,9 %	-14,2 %	-39,2 %	-67,2 %	-28,0 %
	HB	-19,4 %	-13,1 %	-73,8 %	-27,7 %	-14,2 %	-16,0 %	-62,2 %	-28,1 %
#25	LS	-6,6 %	26,3 %	-95,0 %	47,7 %	52,8 %	-89,2 %	-97,1 %	74,0 %
	HB	-6,6 %	25,6 %	-93,1 %	56,3 %	52,8 %	-90,2 %	-97,1 %	83,4 %

Table 7. Distances (in m) between the estimated and the as-built center of curvature.

Element #		GIS CntLine	GPS-IMU Traj	GPS-IMU _CigLine	GPS-IMU _CntLine	GNSS Traj	GNSS LatLine	GNSS CigLine	GNSS CntLine
#5	LS	183,42	115,87	451,01	307,89	n.a.	91,21	538,19	380,16
	HB	183,42	89,98	451,01	307,15	n.a.	81,75	538,19	380,07
#9	LS	6,48	63,30	384,40	59,01	60,18	306,27	390,42	53,60
	HB	6,48	63,30	384,89	55,20	60,15	245,38	388,94	55,43
#13	LS	21,80	17,18	413,77	41,11	26,33	60,40	505,06	40,73
	HB	21,79	23,80	408,06	17,03	26,33	30,68	508,62	33,49
#17	LS	1,29	5,21	22,21	6,36	3,49	1,20	12,36	4,09
	HB	1,28	5,19	12,33	5,39	3,48	1,57	7,27	3,56
#21	LS	107,75	72,98	406,62	161,38	79,34	217,30	371,77	154,96
	HB	107,96	74,48	409,11	154,73	79,34	89,20	343,83	155,58
#25	LS	33,64	129,39	480,38	236,25	263,45	449,23	494,52	369,22
	HB	33,64	126,08	469,24	278,98	263,45	453,99	494,06	416,04

Table 8. Percentage errors of tangent directions.

Element #		GIS CntLine	GPS-IMU Traj	GPS-IMU _CigLine	GPS-IMU _CntLine	GNSS Traj	GNSS LatLine	GNSS CigLine	GNSS CntLine
#3	LS	0,01 %	-0,2 %	4,7 %	-5,2 %	-1,6 %	-0,4 %	-2,6 %	-5,0 %
	HB	0,01 %	-0,2 %	2,2 %	-6,2 %	-1,6 %	-2,0 %	-1,2 %	-6,3 %
#7	LS	0,3 %	0,4 %	0,1 %	0,3 %	0,3 %	0,2 %	0,2 %	0,3 %
	HB	0,3 %	0,4 %	0,09 %	0,3 %	0,4 %	0,3 %	0,2 %	0,3 %
#11	LS	-0,6 %	-0,9 %	6,9 %	-0,5 %	-1,2 %	-0,6 %	0,2 %	-0,6 %
	HB	-0,6 %	-0,8 %	8,7 %	-0,6 %	-1,2 %	-0,6 %	0,2 %	-0,6 %
#15	LS	0,4 %	0,2 %	-0,05 %	0,4 %	0,2 %	0,4 %	-0,2 %	0,3 %
	HB	0,4 %	0,2 %	0 %	0,4 %	0,2 %	0,3 %	-0,2 %	0,3 %
#23	LS	n.a.	7,9 %	n.a.	n.a.	n.a.	n.a.	n.a.	n.a.
	HB	n.a.	7,9 %	n.a.	n.a.	n.a.	n.a.	n.a.	n.a.

Table 9. Time and costs for the acquisition and post-processing of the survey techniques used in the investigation.

	Time		Costs		
Technique	**Acquisition ([a])**	**Post-processing ([a])**	**Device ([b])**	**Acquisition ([b])**	**Data treatment ([b])**
Orthophoto (aerial acquisition of stereo pairs of images)	1	4	2-4	2	2
MM with low cost GPS-IMU sensors (terrestrial vehicle equipped with digital camera and Inertial Measurement Units)	1	4	2	3	4
MM with Global Navigation Satellite System - GNSS (terrestrial vehicle equipped with digital camera and GNSS receiver)	1	3	5	4	3

Legend: ([a]) 1 = faster – 5 = slower, ([b]) 1 = cheaper – 5 = more expensive